# Preparation of multi-functionalized $Fe_3O_4$/Au nanoparticles for medical purposes

(Submitted to Colloids and Surfaces B: Biointerfaces)

*María del Mar Ramos-Tejada*[1]*, *Julian L. Viota*[2], *Katarzyna Rudzka*[3] and *Angel V. Delgado*[3]

[1]Department of Physics, University of Jaén, 23700 Linares, Spain

[2]Vircell S.L., Health Sciences Technological Park, 18016 Granada, Spain

[3]Department of Applied Physics, University of Granada, 18071 Granada, Spain

**Corresponding Author**

*María del Mar Ramos

Department of Physics

Polytechnic School

23071 Linares, Jaén, Spain

mmramos@ujaen.es

## ABSTRACT

In this work, we investigate a route towards the synthesis of multi-functionalized nanoparticles for medical purposes. The aim is to produce magnetite/gold ($Fe_3O_4$/Au) nanoparticles combining several complementary properties, specifically, being able to carry simultaneously an antitumor drug and a selected antibody chosen so as to improve specificity of the drug vehicle. The procedure included, firstly, the preparation of $Fe_3O_4$ cores coated with Au nanoparticles: this was achieved by using initially the layer-by-layer technique in order to coat the magnetite particles with a three polyelectrolyte (cationic-anionic-cationic) layer. With this, the particles became a good substrate for the growth of the gold layer in a well-defined core–shell structure. The resulting nanoparticles benefit from the magnetic properties of the magnetite and the robust chemistry and the biostability of gold surfaces. Subsequently, the $Fe_3O_4$/Au nanoparticles were functionalized with a humanized monoclonal antibody, bevacizumab, and a chemotherapy drug, doxorubicin. Taken together, bevacizumab enhances the therapeutic effect of chemotherapy agents on some kinds of tumors. In this work we first discuss the morphology of the particles and the electrical characteristics of their surface in the successive synthesis stages. Special attention is paid to the chemical stability of the final coating, and the physical stability of the suspensions of the nanoparticles in aqueous solutions and phosphate buffer . We describe how optical absorbance and electrokinetic data provide a follow up of the progress of the nanostructure formation. Additionally, the same techniques are employed to demonstrate that the composite nanoparticles are capable of loading/releasing doxorubicin and/or bevacizumab.



## KEYWORDS

Bevacizumab; doxorubicin; drug loading; drug release; magnetite/gold nanoparticles; monoclonal antibody.

## 1. Introduction

One of the main objectives in anticancer drug development is the design of delivery systems that can contribute to transport and release the therapeutic agents in a targeted and selective fashion to their site of action, thus decreasing adverse effects and enhancing efficacy and specificity. Nanoparticles (NPs) have been demonstrated to be a main component of recent strategies aimed at delivering conventional drugs, recombinant proteins, vaccines and, more recently, nucleotides. NPs modify the kinetics, body distribution and release of an associated drug, and can perform this function either passively (the drug is released by diffusion or matrix dissolution in an otherwise uncontrolled way) or actively (specific interactions are established between the NP functional groups and the target cell, which trigger their payload release only in specified conditions [1]). In the first case, NPs-based systems work by exploiting the special characteristics of tumor growth, specifically, the so-called EPR (enhanced permeability and retention) effect [2-4] as a passive form of targeting. As a result of the imperfect (leaky) vasculature and limited lymphatic drainage, EPR favors that nanoparticles smaller than 100 nm can enter the interstitia and be captured by the tumor cells [3, 5, 6]. In active targeting, specific ligands attached to the surface of the drug vehicles allow their binding to receptors over-expressed by tumor cells and not by normal cells [6].

The possibilities of driving the nanoparticles to the site of action and keeping them there during the drug release are enhanced if an external field can be used with that purpose . As an example, a growing interest exists in iron oxide nanoparticles as core of nanostructures which can be responsive to external magnetic fields. Additional advantages of those superparamagnetic

particles in biomedical and clinical applications come from their enormous potential in such techniques as magnetic resonance imaging (MRI) contrast agents [7], magnetic hyperthermia treatment [8, 9] or tissue repair [10]. In spite of such applications, improvements are still needed concerning their biocompatibility, mechanisms of attachment to cells and biomolecules, colloidal and physical stability, or water dispersibility [11]. These modifications are essential for efficient delivery to cells.

A possible modification consists of producing a gold coating prior to loading the resulting composite nanoparticles with its drug payload [12, 13]. Justification for this is related to the fact that gold particles have low toxicity, high surface area, tunable stability, and significant chemical reactivity. Their presence on the magnetic cores may improve their capabilities for adsorbing, transporting and releasing the active chemicals [14, 15]. The resulting magnetic nanostructures would have the additional advantage of particular optical properties, specifically, increased absorbance in the visible spectrum, thus opening the possibility of using them in photothermal therapy.

Doxorubicin (DOX) will be used as drug payload. This is one of the most potent and widely used anticancer drugs, and it works by inhibiting the synthesis of nucleic acids within cancer cells [16]. However, it has a number of well known undesirable side effects such as cardiotoxicity and myelosuppression, leading to a very narrow therapeutic index. For this reason, a number of investigations have focused on ways to deliver DOX to cancer tissues in a controlled way, so as to reduce such side effects. For instance, DOX was conjugated to poly(lactic-co-glycolic) acid (PLGA) nanoparticles and tested in vivo by Yoo et al. [16]. Comparison with daily DOX injections was carried out by Brannon-Peppas and Blanchette [17], who showed a good suppression of tumor growth, comparable to but not better than standard treatment with injected

DOX. In vitro tests have been described by Rudzka et al. [18] and Gómez-Sotomayor et al. [19] using magnetic nanostructures based on superparamagnetic maghemite or iron/magnetite nanoparticles.

Bevacizumab (Avastin®, BEV hereafter), a humanized recombinant monoclonal antibody, is the first anti-angiogenic protein approved by the FDA (USA) as an anti-(human vascular endothelial growth factor) (VEGF) agent. This is a blood circulating protein responsible for blood vessels growth, and up-regulated in numerous benign and malignant disorders, including angiosarcoma, hemangiomas, and solid tumors. BEV has shown antitumor activity in a number of tumor types, especially when combined with standard chemotherapy treatments [20, 21]. Studies of the combination of bevacizumab to anthracycline-based cancer therapy like DOX have found promising results although, in some cases, the combination of DOX and BEV can result toxic [21, 22]. Wang et al. [23] studied the efficiency of a combination therapy of BEV and DOX on T-leukemia/lymphoma, and found that if both compounds are administered simultaneously the therapeutic effect of the drug in the treatment of this malignancy was greatly improved. A similar synergistic effect between DOX and BEV was described by Kim et al. [24] in the treatment of sarcoma patients. Likewise, improvements in the response of breast cancer to the combination of BEV and DOX compared to DOX alone were found by Lindholm et al. [25], whereas Kristian et al. [26] demonstrated that when DOX was given to breast cancer patients 24 h after BEV the drug efficacy was reduced in comparison to concomitant treatment.

In this work we describe the preparation and functionalization of superparamagnetic magnetite nanoparticles, coated with a gold shell, as delivery systems for DOX and BEV. Magnetite nanoparticles were coated with three polyelectrolyte (cationic-anionic-cationic) layers using the layer-by-layer technique [27, 28]. Then a gold layer was added using the same technique. We

discuss the morphology of the particles and the electrical characteristics of their surface in the successive synthesis stages. Special attention is paid to the chemical stability of the final coating, and the physical stability of the suspensions of the nanoparticles in aqueous solutions. Subsequently, we study the possible application of the $Fe_3O_4$/Au nanoparticles as antitumor drug vehicles. The $Fe_3O_4$/Au nanoparticles were functionalized with Bevacizumab and Doxorubicin, and the nanoparticles containing DOX, BEV and DOX+BEV were characterized in terms of zeta potential. Finally, the release profiles of the two compounds, either jointly of separately, were examined.

## 2. Materials and Methods

### 2.1. Materials.

Iron (II) sulfate heptahydrate ($FeSO_4 \cdot 7H_2O$) was purchased from Fluka. Potassium nitrate ($KNO_3$), sodium hydroxide (NaOH), polyethyleneimine (PEI, $M_w \approx$ 2000 g/mol), poly(styrenesulfonate) (PSS, $M_w \approx 2 \cdot 10^6$ g/mol), chloroauric acid ($HAuCl_4$), sodium citrate tribasic dihydrate, sodium borohydride ($NaBH_4$), doxorubicin hydrochloride ($C_{27}H_{29}NO_{11} \cdot HCl$), sodium chloride (NaCl), and hydrochloric acid (HCl) were from Sigma-Aldrich. Bevacizumab (Avastin® 25 mg/ml) was from Genentech/Roche (Hoffmann-la Roche, Basel, Switzerland). All chemicals were used as received with no further purification. Water used in the experiments was deionized and filtered (Milli-Q Academic, Millipore, France).

### 2.2. Synthesis of magnetite nanoparticles.

The $Fe_3O_4$ cores were synthesized by mixing 0.7 g of $FeSO_4$ with 80 ml of distilled water followed by the addition of 10 ml of 2 M $KNO_3$ and 10 ml of 1 M NaOH in an oxygen-free environment at 90 $^oC$ [29]. The resulting magnetic nanoparticles (MNPs) were magnetically separated from the reaction mixture by placing the container on a 500 mT Nd permanent magnet for 10 min. The collected NPs were rinsed and resuspended in Milli-Q water at least three times, and stored in nitrogen-purged Milli-Q water.

### 2.3. Preparation of polymer-coated magnetic nanoparticles.

5 ml of MNP suspension (1 g/l) were mixed dropwise with 5 ml of PEI solution (2 g/l) under ultrasonic agitation. Sonication was applied during 90 min and then the sample was left undisturbed during 30 min. Washing was subsequently performed by magnetically decanting the magnetic nanoparticles and discarding the supernatant. The particles were finally redispersed in 5 ml of water. A second layer of PSS and a third layer of PEI were added following the same concentrations and process conditions.

### 2.4. Synthesis of gold nanoparticles.

Citrate-stabilized, negatively charged gold nanoparticles were synthesized following the method of reduction of chloroauric acid with $NaBH_4$ described in Ref. [30]. Firstly, 0.5 ml of a 0.1 M $NaBH_4$ solution was cooled down inside a vessel with ice. Then, 0.5 ml of 0.01 M $HAuCl_4$ was mixed with 0.5 ml of 0.01 M trisodium citrate solution and added to 18 ml of distilled water and stirring. We added rapidly the 0.5 ml of the cooled $NaBH_4$ solution, while stirring vigorously at

room temperature. This causes the reduction of $Au^{3+}$ ions to neutral gold atoms. After a few seconds, when the solution color turned pink, indicating the formation of gold nanoparticles, stirring was stopped and the synthesis was allowed to stay for 2 h.

### 2.5. Synthesis of gold-modified MNPs (AuMNPs).

In order to deposit gold seeds onto the polymer-coated magnetite, magnetite+PEI+PSS+PEI nanoparticles were dispersed in 20 ml of water up to a particle concentration of 0.25 mg/ml, and the resulting suspension was added dropwise to the gold seeds solution (after dilution by addition of 10 ml of water to 30 ml of the original gold suspension) under sonication. The obtained suspension was sonicated for 15 min, and it was later let to stay for 30 min and cleaned as before. Finally, we redispersed the gold-modified NPs (AuMNPs) in water (2 ml). The final concentration of AuMNPs was 2.5 mg/ml.

### 2.6. Drug loading.

Aqueous drug solutions (0.1 ml) with different concentrations were mixed with an aqueous solution of the final gold coated-particles (1 mg/ml of AuMNps; 0.1 ml) and the mixtures were shaken during at least 48 h at room temperature. After that time, AuMNPs were separated form supernatants by the magnetic decantation procedure described. In order to determine the amount of adsorbed drug, optical absorbance of the supernatants was measured at 489 nm (in the case of DOX) and 270 nm (in case of BEV), and compared to that of the initial drug solution. The spectrophotometer used was a Dinko UV-8500 UV-Vis from Dinko Instruments, Spain.

### 2.7. Drug release.

1 mg of AuMNPs was first kept in contact with 0.2 ml of the drug solutions and maintained during 48 h under shaking. Then the particles were magnetically separated from the supernatant, re-dispersed in the culture medium (0.4 ml) and kept at 37 ºC during the release experiments. At specified time intervals, the particles were decanted by application of the magnet, and 0.18 ml of the supernatant was taken. An equal volume of phosphate buffer was added to the samples and they were shaken before placing then back in the thermostatic bath. The absorbance of supernatants was determined and the concentration of drug in it was calculated.

### 2.8. Electrophoretic mobility measurements.

The electrophoretic mobility measurements were carried out 24 h after preparation of dilute suspensions with fixed ionic strength using a Zetasizer Nano-ZS (from Malvern Instruments, UK). NaOH and HCl were employed to adjust the pH values of the suspensions. The electrophoretic mobility was measured by performing 3 runs of 3 measurement cycles each.

## 3. Results and Discussion

### 3.1. Stability of the polymer layer.

As described, in order to improve the gold particle attachment to magnetite cores, these were coated with several polyelectrolyte layers using the layer by layer technique [27, 28]. The stability of such layers with time was monitored by means of electrophoretic mobility, $u_e$ (Fig. 1). MNPs (both uncoated and coated with the different layers) were redispersed in 1 mM NaCl solutions at different pH values and then, the electrophoretic mobility of the samples was measured at different times Fig. 1.a shows the electrophoretic mobility of PEI-coated MNPs as a function of pH and of aging time. The initial increase in the magnetite mobility towards positive

values, with absence of isoelectric point ($pH_{iep}$, originally at pH ≈ 6), is an indication of the adsorption of PEI. Nevertheless, the mobility trend is clearly modified after 4 days aging, particularly at pH above neutrality. It must be kept in mind that the positive charge of PEI molecules is strongly decreased at such pH conditions (the p$K_a$ values of PEI are ~9 for primary, ~8 for secondary, and 6-7 for tertiary amines on the polymer backbone [31]), and hence it can be expected that the desorption suggested by the data in Fig. 1.a is favorable in the conditions mentioned. This is certainly an apparent drawback of the method, but it can be avoided, in principle, by performing the successive coatings after 24 h or less, as indeed done in this work. The results in Fig. 1.b demonstrate first of all the negative charge of PSS-coated MNPs, as well as the fact that coating with a triple layer (PEI-PSS-PEI) leads to much more stable nanostructures. It appears that the polyelectrolyte layers intermix in such way that the multilayer adsorption is virtually irreversible. Note that only at pH 7 can some desorption be measured, again due to the proximity of this pH value to the p$K_a$ of PEI.

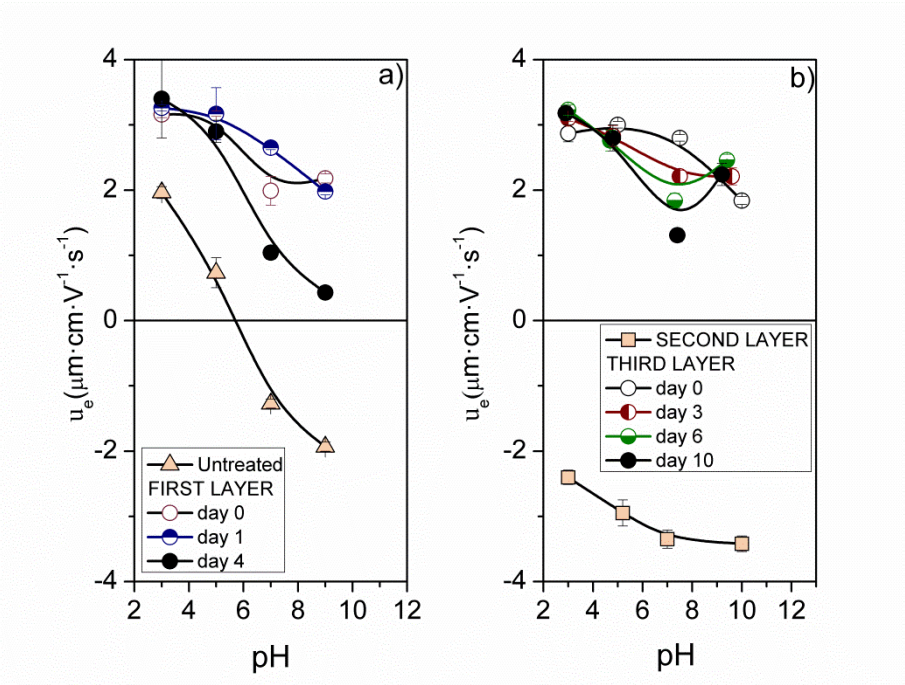


Fig. 1

### 3.2. Characterization of the magnetite-based nanoparticles.

Fig. 2A shows typical high-resolution transmission electron microscope (HRTEM, Philips STEM CM20, The Netherlands) pictures of magnetite nanoparticles with gold seeds on their surface, fabricated using the methods described. This picture illustrates that the gold coating is quite rough but uniform. The size distribution histograms obtained from HRTEM images show that the $Fe_3O_4$ cores have a size of 43 ± 6 nm (average face-centered diagonal) whereas AuMNPs have an average size of 53 ± 9 nm, indicating a roughly 5 nm thick coating. The need of particle size control when designing drug delivery vehicles is well documented: both extravasation of the nanostructures and internalization by cells are optimized for particles in the 10-100 nm size roughly [17, 32, 33], an interval containing the sizes of our nanovehicles.

Keeping in mind that these particles were designed with the aim of eventually driving them to the site of action and maintaining them there by means of magnetic field gradients, it can be understood that the magnetic characterization of the composites is an essential issue. Considering the small size of the magnetite cores, superparamagnetic behavior is expected at room temperature for the nanoparticles synthesized. Fig. 2B shows their magnetization curve at room temperature (obtained in a Quantum Design MPMS XL, USA, Squid magnetometer). No hysteresis is observed, as expected from the superparamagnetic behavior of magnetite cores; however, when a moderate magnetization is reached (about 10 emu/g, or five times smaller than that of magnetite nanoparticles), the typical saturation of the magnetization curve is substituted by a decreasing trend, typical of diamagnetic materials. The presence of the polyelectrolyte layers can account for the rather low maximum magnetization achieved, whereas the high-field decrease must be a consequence of gold nanoparticles displaying diamagnetism, as we can discard the possibility of perturbation of the measurements by the sample holder. In fact, although bulk gold is diamagnetic, gold-based nanostructures have been reported to present a variety of magnetic behaviors, ranging from paramagnetic to ferromagnetic [34, 35]. Experimental data reported by Tuboltsev et al. [34] indicate that, although nanocrystalline gold may exhibit intrinsic ferromagnetism, the structure of deposited clusters on a substrate (as may be the case for our particles on magnetite) may favor the onset of the diamagnetic behavior of bulk gold . It must be mentioned, nevertheless, that the decrease in magnetization below the maximum value reached is not very significant, and hence the particles remain as useful magnetic vehicles for the drug and the antigen.

Concerning the stability of the gold-coated MNPs, HRTEM pictures taken as many as 90 days after preparation do not suggest significant changes, a fact confirmed by $u_e$ measurements (data

not shown for brevity). This structural stability manifests itself in colloidal stability of the nanoparticles. There are several reasons that justify that the particles are rather stable. First, we must consider that the polyelectrolyte coating provides both electrostatic and steric repulsion between the nanoparticles. Second, the magnetic interaction is very weak, as the combination of the small size of the superparamagnetic cores with the diamagnetism of the deposited gold produces a rather small magnetic moment, and the interaction would be further screened by the relatively thick polymer+Au layer. As a result, thermal energy is quite larger than magnetic one, in the absence of applied external field. To these arguments, we must add the electrostatic repulsion between the outermost gold layers.

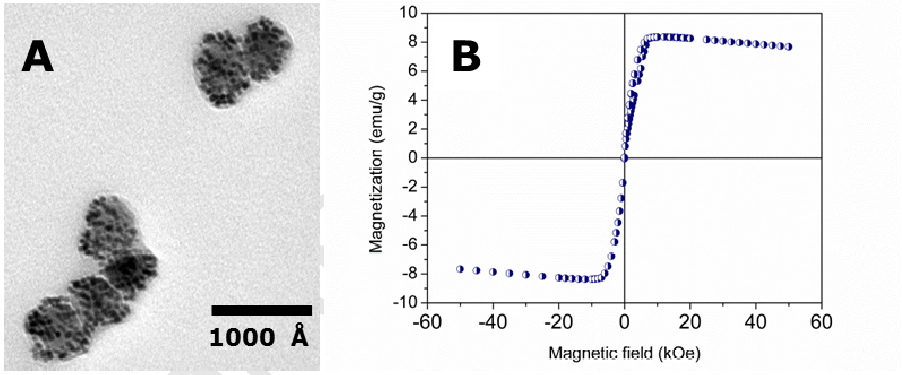


Fig.2

### 3.3. DOX loading and release.

Fig. 3.a shows the adsorption density, $\Gamma$, of DOX on the AuMNPs. Note that the drug adsorption increases with the equilibrium concentration of doxorubicin in solution up to 0.12 mM, where saturation is reached at approximately 5 μmol/g. The results were fitted to the Langmuir isotherm model, $\Gamma = \frac{\Gamma_{max} + kC}{1+kC}$, and the best-fit parameters in our case were $k$ = 0.66 ± 0.25 (l/μmol) and

$\Gamma_{max}$ = 5.3 ± 0.4 μmol/g. The mechanism of DOX binding to nanospheres is likely based on electrostatic interaction between the positive charge of dissolved DOX (through protonation of the amino group of the drug molecule), and the negative surface charge of gold. Adsorption of DOX molecules onto AuMNPs can be further qualitatively followed by electrophoresis. As observed in Fig. 3.b, the change of sign and the further rise of $u_e$ beyond neutralization confirm the incorporation of the drug. Concerning the stability of the drug-coated particles towards aggregation, data in Fig. 3b show that the adsorption of this drug changes the surface charge from negative to clearly positive, so that the electrostatic repulsion still exists after adsorption, and stability is still favored.

Sailor and Park [36] have calculated the payload capacity of solid nanoparticles as a function of nanoparticle diameter. They assumed that the maximum loading is the hexagonal close packed, 74% packing efficiency, with the drug molecules approximated as spheres. Their calculations were performed using both DOX and BEV. They estimated that the number of DOX molecules that can be loaded onto a spherical particle 50 nm in diameter is more than 2000. If we consider our AuMNPs spheres with 53 nm diameter and the value of $\Gamma_{max}$ above reported, we can estimate that the number of DOX molecules loaded onto AuMNP is around 1220 molecules/particle.

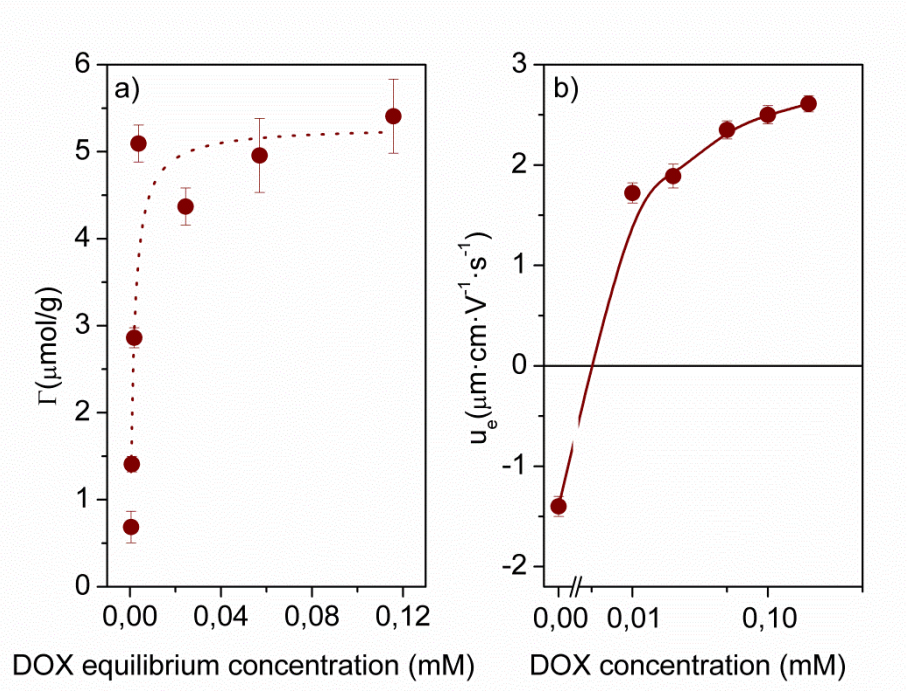


Fig. 3

The kinetics of DOX release is plotted in Fig. 4. Note that almost 80% of the drug adsorbed is released after 50 h. As in other release systems, the kind of kinetics gives us clues concerning the mechanisms of drug discharge from the nanovehicle. It is out of the scope of this article to perform an exhaustive analysis of the best-fit kinetic curve, so we used a general one, the Weibull model [37], according to which, the released amount can be written:

$$Q(t) = Q_\infty - (Q_\infty - Q_0)\exp\left[-(kt)^d\right]$$

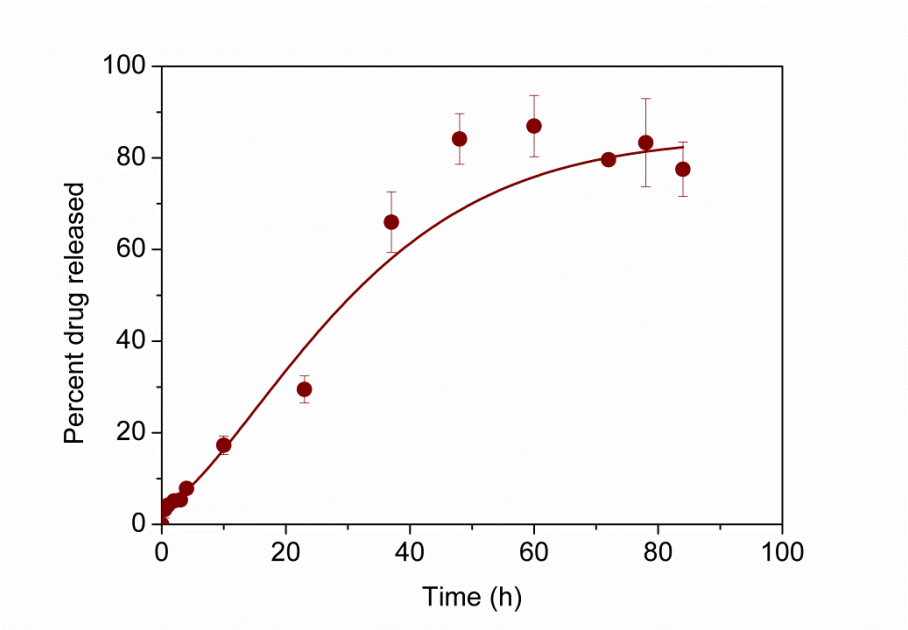


Fig. 4

where $Q_\infty (Q_0)$ is the amount released at long(short) time, $1/k$ is an indication of the time scale of the process, and $d$ controls the shape of the curve. The fitting of the data in Fig. 4 yields a characteristic release time of 34 ± 6 h, with an adjusted determination coefficient $r^2 = 0.993$. If the assumption of electrostatic attraction as mechanism of adsorption is correct, we can expect a behavior of the type known as *environment responsive systems.* In our case, the pH of the medium will be the driving force, since at the pH of the release medium (7.4) the average positive charge of the DOX molecules is reduced by its proximity to p$K_a$, and hence the DOX-AuMNPs attraction is weakened. In addition, the ionic strength of the medium also contributes to such a reduction due to increased screening. As a result, diffusion is the only plausible (passive) mechanism of release in our case. Finally, concerning the characteristic release time, it appears well suited for drug delivery purposes, since maximum plasmatic concentrations remain during almost two days.

### 3.4. BEV loading and release.

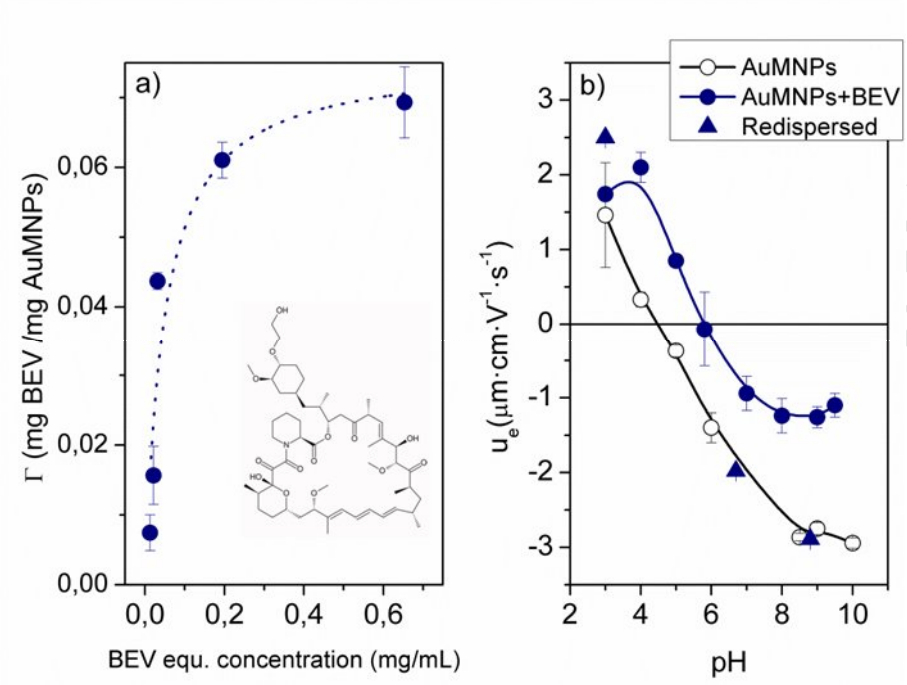


Fig 5

Fig. 5.a shows the adsorption density of BEV on the AuMNPs. Langmuir-type adsorption behaviour is observed with isotherm parameters $k$ = 21 ± 10 (l/mg), $\Gamma_{max}$= 0,076 ± 0.011 mg/mg. The existing information on the charge of BEV molecules is scarce, and it has been suggested that it is small and negative at pH 7.4 [38]. This means that electrostatic interactions can be practically ruled out, as they are likely repulsive, if existent at all. From the molecular structure of BEV included in Fig. 5.a hydrophobic attraction is suggested as the main reasonable mechanism. It can be estimated that around 114 BEV molecules are absorbed on each AuMNP particle, comparable to the value of 150 reported by Sailor and Park [36].

As before, we have used electrophoretic mobility data as a further test of the surface coating. This is done in Fig. 5.b through the comparison of $u_e$ for AuMNPs, both raw and BEV-loaded,

314 with that shown by the latter particles after 24 h contact with a 1 mM NaCl solution. In spite of
315 its significant adsorption , the effect of BEV on the mobility is very limited. However, it can be
316 expected that its comparatively large size must compensate the presumably lower electrostatic
317 repulsion with an increased steric one. As a result, no tendency was observed towards
318 aggregation when BEV were added.

319 Interpretation of mobility data requires some knowledge about the expected pH dependence of
320 the charge of BEV, mostly at physiological conditions. As mentioned, Li et al. [39] concluded
321 that BEV molecules bear a small negative charge at pH 7.4 and 0.16 M ionic strength, whereas
322 Andrew et al. [38] mention a $pH_{iep}$ of 7.6, so that the charge would be slightly positive at the
323 conditions mentioned. This means that at pH 7.6 and above, electrostatic repulsion between BEV
324 and AuMNPs will favor desorption, explaining the tendency of the mobility curve of BEV-
325 loaded particles to that of bare AuMNPs at basic pH values, and not so in acid conditions (Fig.
326 5.b). The kinetics of BEV release is plotted in Fig. 6. Note that, as expected, the strength of the
327 interactions between BEV molecules and the AuMNPs is rather weak: using the same Weibull
328 kinetics as in the case of DOX (line in Fig. 6), it is found that almost 50% of the antigen is
329 released within the first 2 hours.

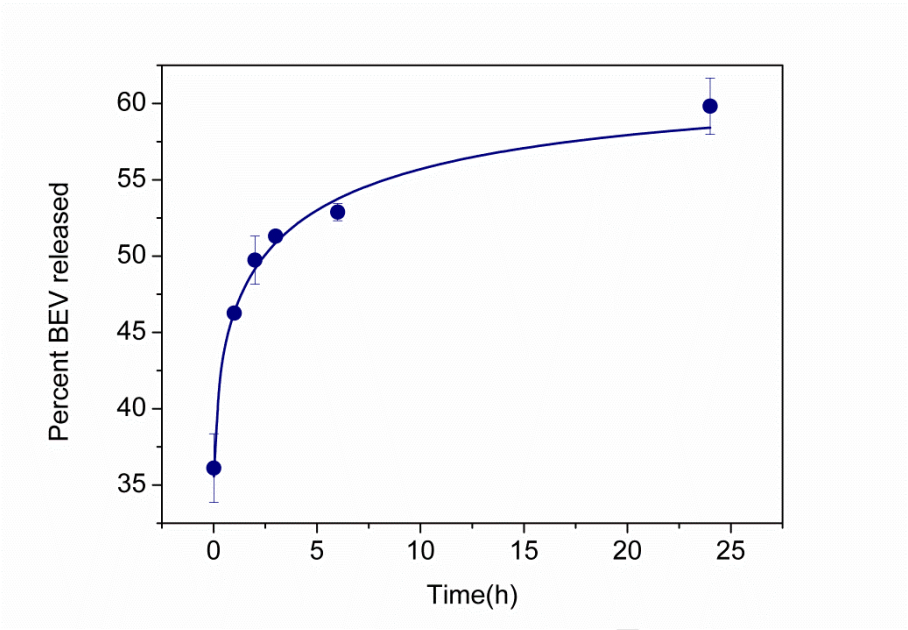


330

331 Fig. 6

332

333 **3.5. Joint loading and release of DOX and BEV.**

334 Fig. 7 shows the adsorption density of DOX and BEV from a solution containing both active
335 agents: in these experiments the concentration of DOX was kept constant at 0.046 mM, and the
336 BEV concentration in solution was changed between 0 and 1 mg/ml. Competitive adsorption is
337 clearly manifested: the adsorption of DOX decreases when BEV concentration is increased,
338 unlike BEV adsorption itself. It appears that BEV occupies adsorption sites mainly because of its
339 possible charge at the pH (~6) of the experiments. Its large molecular size prevents DOX of
340 reaching those available sites hidden by BEV. Nevertheless, there is still significant adsorption
341 of both kinds of molecules, although reduced by about 50% (DOX) and 25% (BEV) as compared
342 to values corresponding to independent adsorption. The competition between the drug and the
343 antigen can also be qualitatively monitored by electrophoresis: Fig. S1 shows that the presence

of DOX does not interfere with the tendency of the mobility to decrease with BEV concentration. The effect of the drug is very significant because of its positive charge, and only in the absence of DOX do we find an isoelectric point for BEV. Note also that at very low BEV concentration, the mobility is positive even in absence of DOX. This is not expected in view of the molecular structure of the antigen, so we can propose that BEV coats the gold particles leaving exposed only the outermost polyelectrolyte layer (i.e., the positive PEI chains).

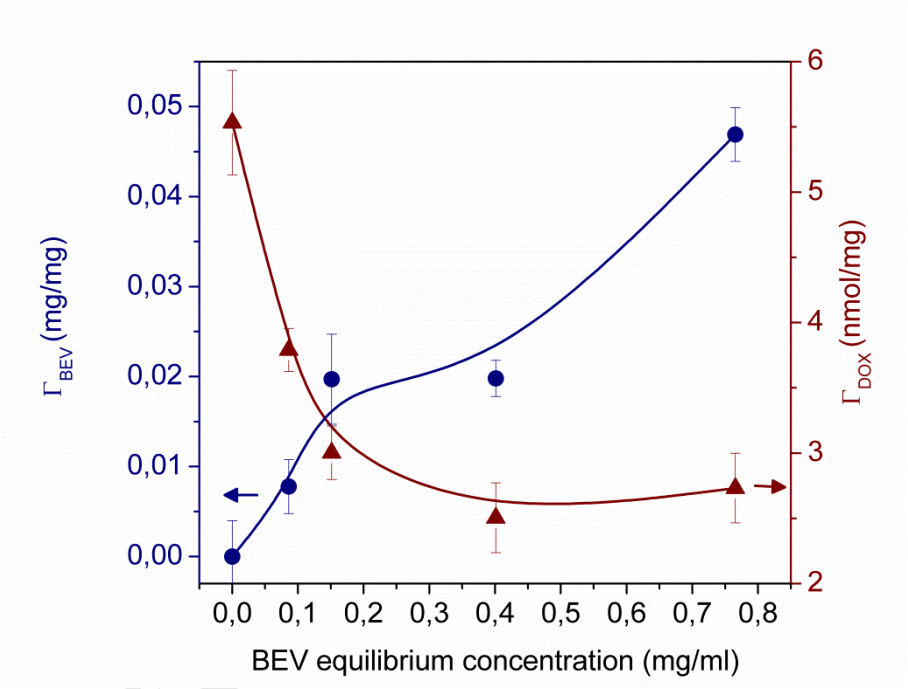


Fig. 7

In this discussion it is also important to consider if the order of incorporation of the drugs onto the AuMNPs has any influence on the adsorption/desorption processes, and in the "which molecule is displaced by which" evaluation. Some information on this can be obtained by measuring the electrophoretic mobility of the particles as a function of DOX concentration in four cases: no BEV added, simultaneous addition of BEV (0.25 mg/ml) and DOX, BEV first and DOX first. The results appear in Fig. S2: it is found that the mere addition of the amount of BEV

358 mentioned controls the mobility whatever the concentration of DOX up to 0.1 mM: the
359 constancy of $u_e$ with the increase of drug in solution confirms that DOX has limited access to
360 adsorption sites always apparently occupied by the (much less charged) BEV molecules. Only at
361 high concentration of DOX can we observe the increase of $u_e$ parallel to that attained without
362 antigen. In any case, the order of addition is irrelevant.

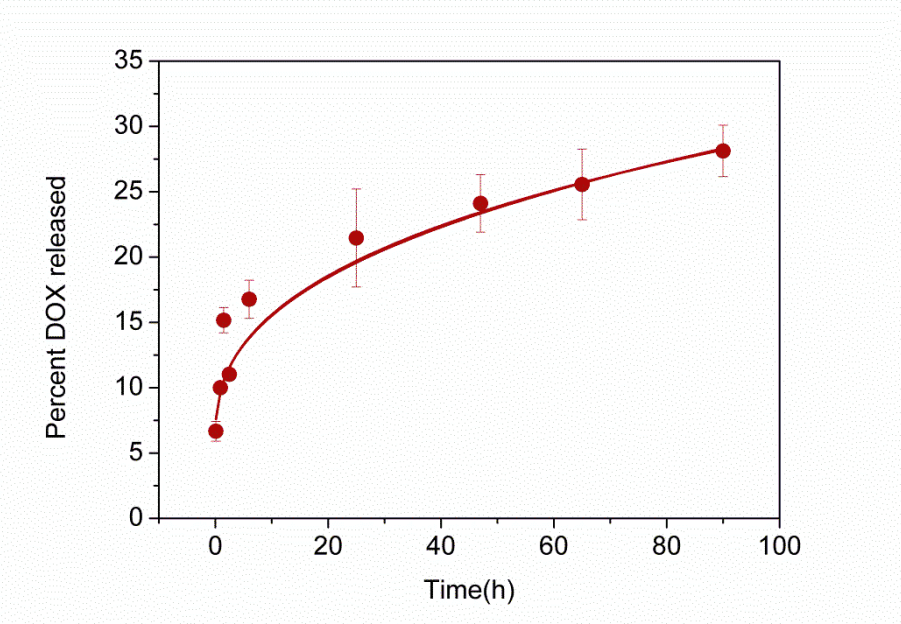


363

364 **Fig. 8**

365 The drug release from the particles loaded with both compounds is illustrated in Fig. 8. It can be
366 observed that the rate of DOX release is much slower in the presence of BEV (compare the fitted
367 characteristic time in Fig. 8, 200 h to reach 50 % release, with that in Fig. 4, 34 h), suggesting
368 that DOX may be trapped in the BEV moieties. On the contrary, although BEV release is much
369 more difficult to follow spectrophotometrically, it was found (results not shown) that the antigen
370 is released even more rapidly (more than 50 % after 6 h), as a consequence of the weak
371 interaction expected between the low-charge BEV molecules and the surface sites, as well as the

likely repulsion exerted by adsorbed DOX. It may hence be presumed that the initially (during the first 10 h in Fig. 8) released DOX corresponds to the drug molecules attached to BEV being liberated with the antigen The two agents hinder their final release and some BEV and a considerable amount of DOX will be available in solution only after longer times. Although it appears that the adsorption-release processes are more favorable if both agents are used separately, the performance of the mixed vehicles is still non-negligible, and deserves to be further explored.

## 4. Conclusions

Multi-functionalized magnetite/gold nanoparticles were synthesized and investigated as mono/multi-drug delivery systems for doxorubicin and bevacizumab. The first step in the preparation of $Fe_3O_4$/Au nanoparticles was achieved using the layer-by-layer technique in order to coat the magnetite particles with a three polyelectrolyte (cationic-anionic-cationic) layer. The polyelectrolyte multilayer formation improves the stability of the coating as compared to a single layer of polyelectrolyte . With this, the particles became a good substrate for the growth of the gold layer in a well-defined core–shell structure. The prepared magnetite/gold nanoparticles are able to load DOX and/or BEV after contact with their solutions. The efficiency of the nanoparticles in adsorbing and releasing the drugs was followed by means of optical absorbance and electrophoretic mobility measurements. We have shown that BEV competes with DOX when they adsorb onto AuMNPs surfaces. The drug and antigen can be simultaneously released from the particles loaded with both compounds although both the amount and rate of any of the released compounds is altered by its interaction with the other. The methods used in this work

for the evaluation of the amount of either drug or BEV adsorbed and released are classical spectroscopic ones, which are well established. When only one adsorbent is considered, the methods are precise enough as long as the molecules have well defined absorbance bands. In our case, the presence of two molecules at the same solution makes the individual detection of adsorbed/desorbed amounts more complicated. This problem must be considered in future work on the subject: specific immunological methods for the detection of BEV must be implemented instead of colorimetric ones.

**ACKNOWLEDGEMENT**

Financial support from Junta de Andalucía (PE2012-FQM0694), and Ministerio de Economía y Competitividad (FIS2013-47666/C3-1-R), Spain, is gratefully acknowledged.

**FIGURE CAPTIONS**

Fig. 1. Electrophoretic mobility of a) PEI-coated NPs, and b) PEI-PSS-PEI core/shell MNPs as a function of pH at different aging times. Ionic strength: $10^{-3}$ M NaCl. Error bars represent the standard deviation of nine determinations.

Fig. 2. A) HRTEM pictures magnetite nanoparticles with gold seeds on their surface. B) Magnetization curve of the same particles.

Fig. 3.a) Adsorption density of DOX on AuMNPs, as a function of equilibrium drug concentration. The line is the best-fit to the Langmuir isotherm. The error bars correspond to half the dispersion of the data after three determinations. b) Electrophoretic mobility of AuMNPs

416 after 24 h contact with doxorubicin solutions of the concentrations indicated, at natural pH and in
417 $10^{-3}$ M NaCl. Error bars represent the standard deviation of nine determinations.
418 Fig. 4. Kinetics of DOX release from magnetic nanoparticles in culture medium at 37 $^{o}$C. The
419 line is the best-fit to a Weibull kinetics. The error bars correspond to half the dispersion of the
420 data after three determinations.
421 Fig. 5.a) Adsorption density of BEV on AuMNPs, as a function of antigen equilibrium
422 concentration. The line is the best-fit to the Langmuir isotherm. A BEV molecular scheme is
423 included. The error bars correspond to half the dispersion of the data after three determinations.
424 b) Electrophoretic mobility of AuMNPs particles as a function of pH before and after 24 h
425 contact with a 0.2 mg/ml BEV solution. Triangles correspond to data obtained by magnetically
426 decanting the corresponding suspensions in BEV solution, and redispersing the solids in the base
427 solution, at the indicated pH. Ionic strength: $10^{-3}$ M NaCl. Error bars represent the standard
428 deviation of nine determinations.
429 Fig. 6. Kinetics of BEV release from magnetic nanoparticles in culture medium at 37$^{o}$C. The line
430 is the best-fit to a Weibull kinetics. The error bars correspond to half the dispersion of the data
431 after three determinations.
432 Fig. 7. Adsorption density of BEV (circles) and DOX (triangles) on AuMNPs as a function of
433 equilibrium BEV concentration. DOX concentration in all cases 46 μM, pH 6. The error bars
434 correspond to half the dispersion of the data after three determinations.
435 Fig.8. Kinetics of DOX release from magnetic nanoparticles in culture medium at 37$^{o}$C. The
436 particles are coated with both compounds (BEV 1 mg/ml and DOX 0.046 mM). The line is the
437 best-fit to a Weibull kinetics. The error bars correspond to half the dispersion of the data after
438 three determinations.

## REFERENCES


[1] S. Parveen, R. Misra and S.K. Sahoo, Nanomed.-Nanotechnol. Biol. Med., 8 (2012) 147.

[2] H. Maeda, H. Nakamura and J. Fang, Adv. Drug Deliver. Rev., 65 (2013) 71.

[3] H. Maeda, G.Y. Bharate and J. Daruwalla, Eur. J. Pharm. Biopharm., 71 (2009) 409.

[4] H. Maeda, T. Sawa and T. Konno, J. Control. Release, 74 (2001) 47.

[5] J.D. Byrne, T. Betancourt and L. Brannon-Peppas, Adv. Drug Deliv. Rev., 60 (2008) 1615.

[6] F. Danhier, O. Feron and V. Préat, J. Control. Release, 148 (2010) 135.

[7] J.E. Rosen, L. Chan, D. B. Shieh and F.X. Gu, Nanomed.-Nanotechnol. Biol. Med., 8 (2012) 275.

[8] I. Hilger, Int. J. Hyperther., 29 (2013) 828.

[9] T. Kobayashi, Biotechnol. J, 6 (2011) 1342.

[10] T. Kito, R. Shibata, M. Ishii, H. Suzuki, T. Himeno, Y. Kataoka, Y. Yamamura, T. Yamamoto, N. Nishio, S. Ito, Y. Numaguchi, T. Tanigawa, J.K. Yamashita, N. Ouchi, H. Honda, K. Isobe and T. Murohara, Sci. Rep., 3 (2013) 1418.

[11] Q.A. Pankhurst, J. Connolly, S.K. Jones and J. Dobson, J. Phys. D. Appl. Phys., 36 (2003) R167.

[12] M. Bikram, A.M. Gobin, R.E. Whitmire and J.L. West, J. Control. Release, 123 (2007) 219.

[13] G.F. Paciotti, D.G.I. Kingston and L. Tamarkin, Drug. Develop. Res., 67 (2006) 47.

[14] E.E. Connor, J. Mwamuka, A. Gole, C.J. Murphy and M.D. Wyatt, Small, 1 (2005) 325.

[15] P. Ghosh, G. Han, M. De, C.K. Kim and V.M. Rotello, Adv. Drug Deliver. Rev., 60 (2008) 1307.

[16] H.S. Yoo, K.H. Lee, J.E. Oh and T.G. Park, J. Control. Release, 68 (2000) 419.

[17] L. Brannon-Peppas and J.O. Blanchette, Adv. Drug Deliver. Rev., 56 (2004) 1649.

[18] K. Rudzka, J.L. Viota, J.A. Munoz-Gamez, A. Carazo, A. Ruiz-Extremera and A.V. Delgado, Colloids Surf., B, 111 (2013) 88.

[19] S. Gómez-Sotomayor, S. Ahualli, J.L. Viota, K. Rudzka and A.V. Delgado, J. Nanosce. Nanotechnol., 14 (2014) 1.

[20] T. Shih and C. Lindley, Clin. Ther., 28 (2006) 1779.

[21] A.T. Stopeck, J.M. Unger, L.M. Rimsza, M. LeBlanc, B. Farnsworth, M. Iannone, M.J. Glenn, R.I. Fisher and T.P. Miller, Blood, 120 (2012) 1210.

[22] D.R. D'Adamo, S.E. Anderson, K. Albritton, J. Yamada, E. Riedel, K. Scheu, G.K. Schwartz, H. Chen and R.G. Maki, J. Clin. Oncol., 23 (2005) 7135.

[23] L. Wang, W.-Y. Shi, F. Yang, W. Tang, G. Gapihan, M. Varna, Z.-X. Shen, S.J. Chen, C. Leboeuf, A. Janin and W.L. Zhao, Haematol.-Hematol. J., 96 (2011) 927.

[24] Y.J. Kim, H.J. Lee, T.M. Kim, T.S.K. Eisinger-Mathason, A.Y. Zhang, B. Schmidt, D.L. Karl, M.S. Nakazawa, P.J. Park, M.C. Simon and S.S. Yoon, Int. J. Cancer, 132 (2013) 29.

[25] E.M. Lindholm, A. Kristian, H. Nalwoga, K. Krüger, S. Nygård, L.A. Akslen, G.M. Mælandsmo and O. Engebraaten, Mol. Oncol., 6 (2012) 418.

[26] A. Kristian, M.E. Revheim, H. Qu, G.M. Maelandsmo, O. Engebraten, T. Seierstad and E. Malinen, Acta Oncol., 52 (2013) 1566.

[27] F. Caruso, Top. Curr. Chem., 227 (2003) 145.

[28] T.Y. Chen and P. Somasundaran, J. Am. Ceram. Soc., 81 (1998) 140.

[29] I.Y. Goon, L.M.H. Lai, M. Lim, P. Munroe, J.J. Gooding and R. Amal, Chem. Mater., 21 (2009) 673.

[30] B.D. Busbee, S.O. Obare and C.J. Murphy, Adv. Mater., 15 (2003) 414.

[31] K. Kim, J.W. Lee, J.Y. Choi and K.S. Shin, Langmuir, 26 (2010) 19163.

[32] G. Storm, S.O. Belliot, T. Daemen and D.D. Lasic, Adv. Drug Deliv. Rev., 17 (1995) 31.

[33] H. Oshima and K. Makino (Eds.), Colloid and Interface Science in Pharmaceutical Research and Development, Elsevier B.V., Oxford, 2014, Chapter 21.

[34] V. Tuboltsev, A. Savin, A. Pirojenko, J. Raisanen, Acs Nano, 7 (2013) 6691.

[35] G.L. Nealon, B. Donnio, R. Greget, J.-P. Kappler, E. Terazzi, J.-L. Gallani, Nanoscale, 4 (2012) 5244.

[36] M.J. Sailor and J.H. Park, Adv. Mater., 24 (2012) 3779.

[37] P. Costa, J. Manuel and S. Lobo, Eur. J. Pharm. Sci., 13 (2001) 123.

[38] J.S. Andrew, E.J. Anglin, E.C. Wu, M.Y. Chen, L. Cheng, W.R. Freeman and M.J. Sailor, Adv. Funct. Mater., 20 (2010) 4168.

[39] S.K. Li, M.R. Liddell and H. Wen, J. Pharm. Biomed. Anal., 55 (2011) 603.

500 **GRAPHICAL ABSTRACT**

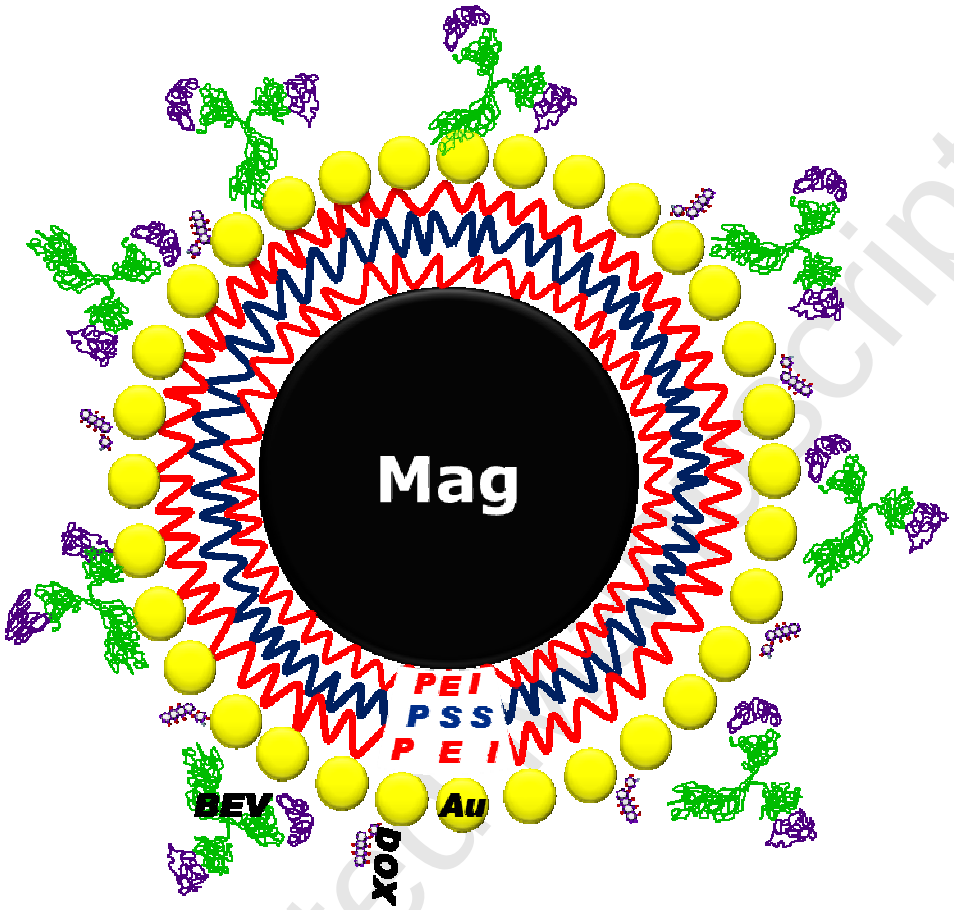


501

502 Competitive BEV and DOX adsorption on the Au-PEI-PSS-PEI magnetic nanoparticles.

503

504

- The preparation of magnetite/gold nanoparticles is described
- A polyelectrolyte multilayer is adsorbed on the magnetic core prior to gold coating
- The polyelectrolyte multilayer formation improves the stability of the coating
- The magnetite/gold nanoparticles are able to load DOX and/or BEV
- The DOX and BEV can be simultaneously released from the particles